

Photodetection of modulated light of white RGB LEDs with a-SiC:H device

Paula Louro^{1,2}, Manuela Vieira^{1,2,3*}, Manuel A. Vieira^{1,2}, J. Costa^{1,2}

¹Electronics Telecommunication and Computer Dept. ISEL/IPL, R. Conselheiro Emídio Navarro, 1949-014 Lisboa, Portugal

²CTS-UNINOVA, Quinta da Torre, Monte da Caparica, 2829-516, Caparica, Portugal.

³DEE-FCT-UNL, Quinta da Torre, Monte da Caparica, 2829-516, Caparica, Portugal Instituto de Telecomunicações,

*Corresponding author

DOI: 10.5185/amp.2018/410

www.vbripress.com/amp

Abstract

We propose the use of Visible Light Communication (VLC) for localization services and navigations. The proposed lighting system supplies the dual function of lighting and data transmission. It uses commercial RGB white LEDs for the generation of the light and of the modulated optical signals that are transmitted in free space using an on-off coding scheme. The red, green and blue emitters of white LEDs are independently modulated, transmitting each different information. The photodetector is a multilayered device based on a-SiC:H, designed for the detection of visible optical light. The generated electrical signal by the photodetector is strictly related to the input optical excitation and its demodulation and decode enables the identification of the input light signals that carry the information necessary to perform the positioning and navigation tasks. The photodetector works as an active optical filter presenting self-amplification at selectable wavelengths. It is a multilayered device composed by two stacked pin photodiodes fabricated between conductive transparent electrical contacts. The positioning system includes multiple, identical navigation cells. The decoded signal by the photodetector identifies the input emitter cell and supplies enhanced accuracy within the spatial region covered by the cell. The methodology used for the photocurrent signal processing involves Fourier transform analysis for frequency identification and the use of a photodetector with spectral selective properties of wavelength identification. An algorithm to decode the information is established and the positioning accuracy is discussed. The experimental results, confirmed that the proposed VLC architecture is suitable for the intended application. Copyright © 2018 VBRI Press.

Keywords: a-SiC: H technology, LED, visible light communication, photodetector, optical sensor, positioning.

Introduction

Visible Light communication (VLC) constitutes a data communications technology based on the use of visible light between 400 and 750 nm [1,2]. These optical communication systems use LEDs to encode and transmit the signals. Currently this achievement is possible due to enormous advances in LED technology, that allow these devices to become cheaper, more powerful and energetically efficient. Due to its characteristics, LEDs can be switched very fast to produce modulated light in high frequencies, allowing data transmission in high speed. Consequently, this free-space, line of sight communication technology aims to address the growing need for energy saving and speed network data transmission. As the technology is mainly related to energy saving lighting sources it uses mostly white LEDs [3], either based on blue emitter coated with a phosphor layer or based on tri-chromatic emitters. The last ones, are more expensive but provide additional bandwidth as three communication channels can be used by independent modulation of the emitters. However, in a few applications e.g. communications, monochromatic LEDs operating at specific wavelengths can be used.

For the detection of the optical signals VLC systems usually include semiconductor photodetectors, generally based on silicon, that supply an optimized response in the visible region of the electromagnetic spectrum due to suitable spectral sensitivity, high quantum efficiency and small size.

Several applications of VLC systems are currently being developed, spanning from low data rate applications such as indoor positioning and navigation to more demanding bandwidth applications like multimedia streaming or internet access points [4, 5].

In this paper we propose the use of a multilayered a-SiC:H [6] device to perform the photodetection of the optical signals generated by white trichromatic RGB LEDs [7, 8]. The system was designed for navigation purposes [9, 10], and the emitters of each white LED were specifically modulated at precise frequencies and coding bit sequences [11, 12]. As the pin photodetector works as an active optical filter, in the visible part of the electromagnetic spectrum, the sensitivity can be externally tuned by using adequate optical bias. This intrinsic device property light wavelength discrimination

and supplies decode tools for the identification of the input signals.

The proposed lighting and positioning/navigation system involves wireless communication, computer based algorithms, smart sensor and optical sources network, which constitutes a transdisciplinary approach framed in cyber-physical systems.

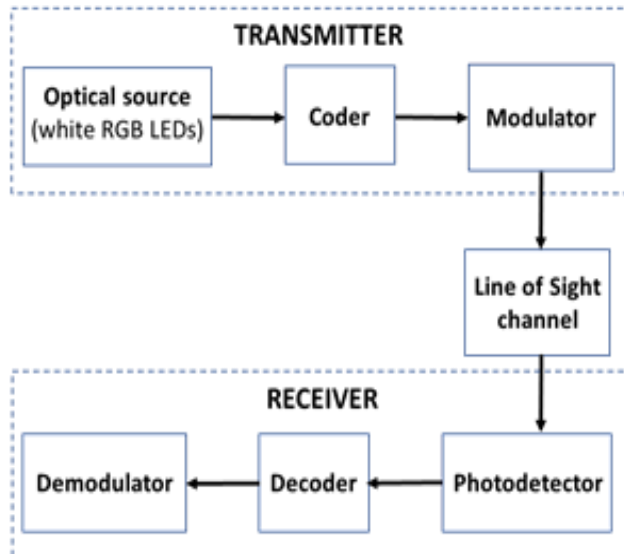


Fig. 1. Block diagram of the visible light communication system.

System design

The proposed VLC system mainly consists of a transmitter that codes the information and modulates the light produced by the emitters embedded in the white RGB LEDs and a receiver with a photosensitive element that extracts the modulated signal from the transmitted light and decodes information through a dedicated algorithm for data analysis. The transmitter and the receiver are physically separated from each other, but connected through the VLC channel, which requires the line of sight condition (Fig. 1). In this case the transmission channel is the atmosphere.

Emitters - transmitter module

The transmitter proposed in this VLC system uses ceiling lamps based on commercial white LEDs, with red, green and blue emitters (w-RGB LEDs). The peaks wavelengths of each w-LED are centered at 464 nm, 535 nm and 630 nm. The luminous intensity of each emitter is regulated by the driving current for white perception by the human eye and the divergence angle is around 120°.

Each ceiling is composed by four white LEDs framed at the corners of a square. Each lamp with this configuration constitutes a navigation unit cell (Fig. 2a). In a real system, several navigation unit cells will be used for lighting and data transmission. Each navigation cell is assigned to different spatial regions covered by the illumination pattern supplied by the LEDs (Fig. 2b).

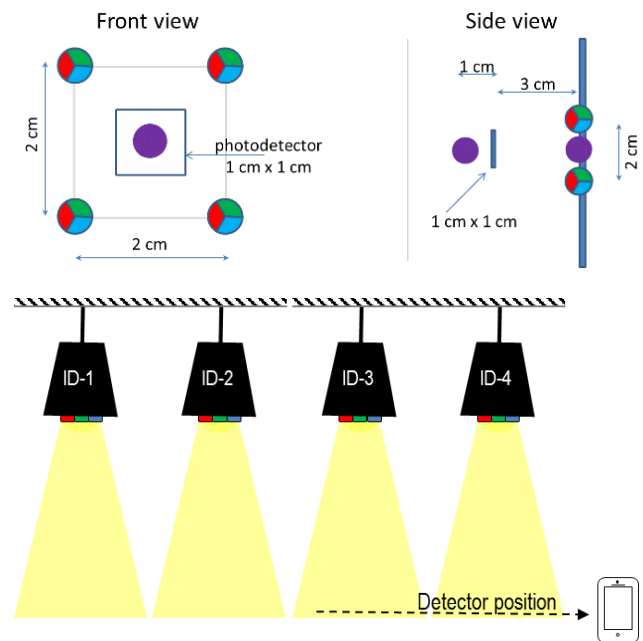


Fig. 2. Configuration of the (a) unit navigation cell and (b) experimental setup with adjacent navigation cells.

The coder converts data into a modulated optical message to be transmitted by each w-LED. The driving current of each emitter is controlled independently supplying the respective coding sequence and frequency. An on-off keying modulation scheme was used with a 16-bit codification, (1: light on and 0: light off).

Photodetector – receiver module

The receiver is the sub-system at the reception end of the communication link that extracts information from the transmitted, modulated light beam. It transforms the light into an electrical signal that is demodulated and decoded. Fig. 3 shows the semiconductor configuration used as integrated photodetector and tunable filter device. It is a monolithic heterojunction composed by two pin structures based on a-Si:H and a-SiC:H built on a glass substrate and sandwiched between two transparent electrical contacts. The device was fabricated by PECVD at 13.56 MHz radio frequency.

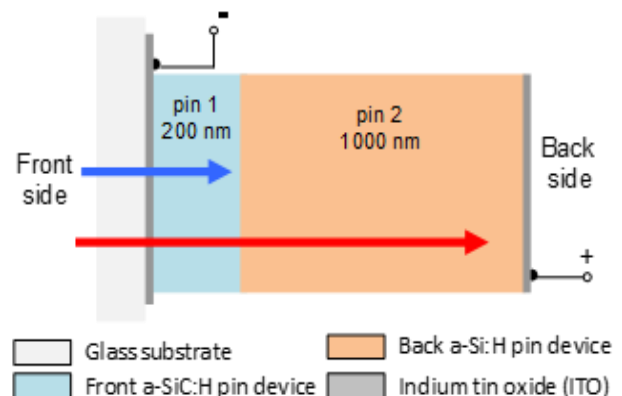


Fig. 3. Configuration of the photodetector at the receiver module.

The intrinsic absorber materials were designed to confer the ability to detect separately short and long visible wavelengths. This assumption led to the engineering design of both intrinsic layers in what concerns thickness and material optical absorption coefficients, resulting in the choice of a narrow (200 nm) high bandgap (2.1 eV, a:SiC:H) material for the front layer and a thicker (1000 nm) lower (1.8 eV, a-Si:H) bandgap semiconductor for the back structure. Thus, the front p-i-n structure (pin1) exhibits high absorption to the blue light (shorter wavelengths) and high transparency to the red wavelength while the back structure (pin2) high absorption of the red wavelength.

In Fig. 4 it is displayed the photodetector transient photocurrent under light produced by the blue, green and red emitters. In this experiment, each emitter was electrically modulated by a rectangular impulse generating a rectangular optical impulse on the device front side. The photocurrent was measured using steady state background monochromatic light (400 nm, violet) from the front and back sides and without optical bias.

Results show that under back violet background illumination the gain is high at short wavelengths (blue light) and decreases for longer wavelengths (green and red). The device behaves as a short-pass filter. Under front violet background light, the device works as a long-pass filter for wavelengths above 500 nm, blocking the shorter wavelengths. The shift of the irradiation device side (front/back) allows tuning the short- and long-spectral regions, while the medium region (475 nm - 530 nm) can only be tuned by using both active filters. Under front illumination the red part of the spectrum is enhanced while under back illumination the main enhancement occurs for the blue signal. The quantification of the signal amplification under front and back bias is determined by the optical gain (α_F and α_B for the front and back gains, respectively), defined at each wavelength (λ) as the ratio between the signal magnitudes measured with and without optical bias. For the red, green and blue light the front optical gain under violet background light is, respectively, 5, 3.5 and 1.3, while for the back optical gains, the values are 0.6, 0.6 and 1.7.

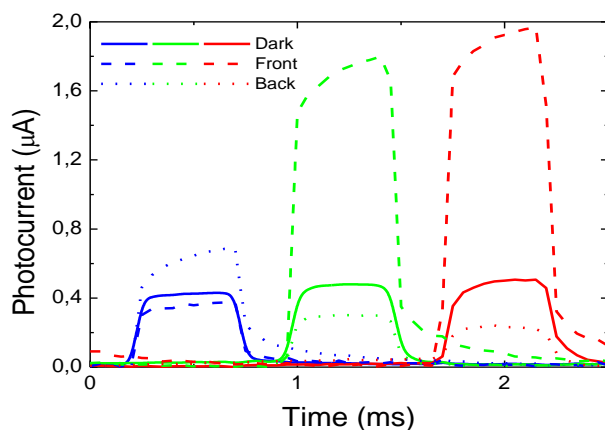


Fig. 4. Photodetector transient photocurrent under light produced by the blue, green and red emitters without optical bias and under front and back optical bias.

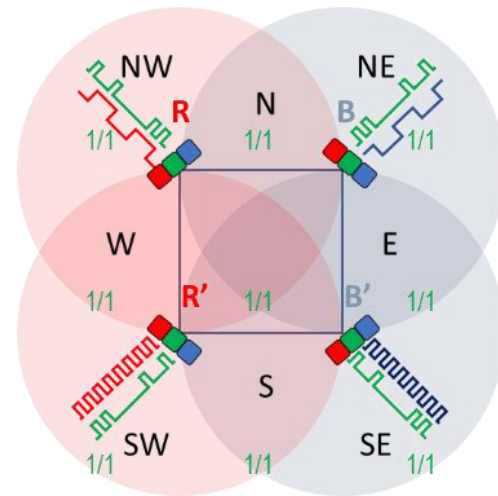


Fig. 5. Configuration of the unit navigation cell showing the emitters (wavelength and frequency) and the cardinal directions assigned to the respective spatial region.

Improved navigation accuracy

In each navigation unit cell, the green emitters of the four white LEDs are modulated with a specific 8-bit sequence coded with the credentials of the position (line and column) assigned to the cell. Therefore, the spatial region of each navigation cell can be easily decoded by the reading out of the photocurrent generated by each navigation signal at the receiver. This supplies a position accuracy related to the area covered by each lamp ceiling unit, which is around: 1.3 m x 1.3 m. For most navigation applications, this value is quite coarse, requiring a severe improvement for better performance. To accomplish this need, additional modulation of the blue and red emitters was also used. The modulation scheme included the red emitters on the left side and the blue emitters of the right side. The top emitters (either red and blue) were operated at a lower frequency than the bottom ones (Fig. 5). Hence, cardinal directions can be assigned to the optical signals generated within the navigation unit cell. The West cardinal direction and the ordinal directions, Northwest and Southwest, are supplied by the red chip of the white LEDs located at the left edge of the square, modulated at different frequencies. East, Northeast and Southwest by the blue emitters, while North and South by both blue and red emitters operating at the same frequency.

In this research, we will assume that each white LED cone of light overlaps in the central region of the square. In the lateral and corner parts, this intersection is partial due to the radiation patterns superposition of the closest two or three LEDs. Outside the square, distinct optical regions correspond also to different spatial regions, with the presence of a single red or blue signal or of two signals (red and blue, or two red or two blue signals). Consequently, the area covered by the different optical excitations will vary along the navigation unit cell (Fig. 6).

The central region, labeled β results from the overlap of the emitted light from the two red emitters, two blue emitters and four green emitters, while the α region at the

corners holds the optical excitation of three green emitters and two blue and one red, or two red and one blue emitter. At the γ and γ' regions the optical pattern is due to two emitters (two green emitters and two blue or two red emitters or one red and one blue emitter). Regions δ and Δ include the irradiation pattern from one single w-LED, i.e., light from one green emitter and from one red or blue emitter. Regions of the navigation cell not covered by any irradiation pattern, correspond to “dark” regions, where the photodetector will not be able the perceive the position.

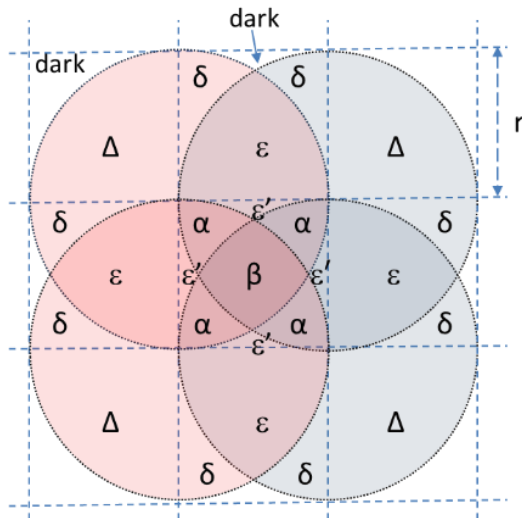


Fig. 6. Diagram of the radiation patterns within each navigation unit cell.

As can be depicted from Fig. 6, the area covered by each irradiation pattern can be evaluated using simple geometrical considerations. This was computed integrating the shadowed area of each region, assuming a circular irradiation flux for each emitter of radius r . Thus,

$$A_\epsilon = 2 \times \int_{r/2}^r \sqrt{r^2 - x^2} \cdot dx \tag{1}$$

$$A_\beta = 4 \left[\int_{r/2}^{\sqrt{3}r/2} \sqrt{r^2 - x^2} dx - r^2 \left(\frac{\sqrt{3}}{2} - \frac{1}{2} \right)^2 \right] \tag{2}$$

Using polar coordinates equations (1) and (2) can be written as:

$$A_\epsilon = 2 \times \int_0^{\pi/3} r^2 \sin^2 \theta \cdot d\theta \tag{3}$$

$$A_\beta = 4 \left(\int_{\pi/6}^{\pi/3} r^2 \sin^2 \theta \cdot d\theta + r^2 \left(1 - \frac{\sqrt{3}}{2} \right)^2 \right) \tag{4}$$

As

$$P \sin^2 x = \frac{1}{2} \cdot (x - \sin x \cos x) + C$$

The solution of equations (3) and (4) is:

$$A_\epsilon = r^2 \left(\frac{\pi}{3} - \frac{\sqrt{3}}{4} \right) \tag{5}$$

$$A_\beta = r^2 \left(\frac{\pi}{12} - 1 + \frac{\sqrt{3}}{2} \right) = 0.315147 \cdot r^2 \tag{6}$$

The evaluation of adjacent areas is given by:

$$A_\delta = \frac{\pi r^2}{4} - A_\epsilon = 0.171213 \cdot r^2 \tag{7}$$

$$A_{\epsilon'} = r^2 - A_\epsilon - 2 \cdot A_\delta = 0.043389 \cdot r^2 \tag{8}$$

$$A_\alpha = \frac{1}{4} (r^2 - A_\beta - 4 \times A_{\epsilon'}) = 0.337418 r^2 \tag{9}$$

Table 1 summarizes the numerical values of each spatial region and the normalized area within the navigation unit cell (assuming an area $3r \times 3r$ for the navigation unit cell).

Thus, the relative areas (compared with the side of the LEDs frame square that constitute the navigation unit cell, Fig. 2a) covered by the different optical excitations within the navigation unit cell are summarized in Table I.

Table 1. Relative area of the irradiation patterns within the navigation unit cell.

Spatial region	Area	Number of regions	Normalized area (navigation unit cell)
ϵ	$0,614185 \cdot r^2$	4	0,272971
δ	$0,171213 \cdot r^2$	8	0,152190
ϵ'	$0,043389 \cdot r^2$	4	0,019284
β	$0,511299 \cdot r^2$	1	0,056811
α	$0,078787 \cdot r^2$	4	0,035016
Δ	$0,785398 \cdot r^2$	4	0,349066
$\Delta + \delta$	$0,956611 \cdot r^2$	4	0,501255
$\epsilon + \epsilon'$	$0,657573 \cdot r^2$	4	0,292255
Dark	$0,214602 \cdot r^2$	4	0,095379

These values allow the evaluation of the accuracy on the determination on the spatial resolution of the positioning system. The dark zones of the navigation unit cell correspond to nearly 10% of the covered area. The region confined to a narrower area is the α region, resultant from the irradiation pattern of three LEDs, followed by the central region (β) where the four LEDs contribute. Regions with poorer resolution are $\epsilon + \epsilon'$ and $\Delta + \delta$, assigned respectively, to optical signals from two and one LEDs.

Results and discussion

Fig. 7 displays the output photocurrent signals, measured with and without front and back optical violet bias, under the influence of a specific navigation unit cell.

In this case, it shown the signals measured by the detector when placed somewhere in the areas labeled Δ/δ , ϵ/ϵ' and β (Fig. 6). The condition, assigned when all optical signals are off, corresponds to the reference level. The single optical signals are displayed at the top of the figure to help the reader with the different on-off optical states.

As can be depicted from Fig. 7 all graphs exhibit sharp peaks assigned to the green emitters, that transmit the signal of the navigation cell identification. Depending on the spatial position, the remaining part of the signals is different. The photocurrent measured under front optical bias (cyan line) takes the highest values, due to the presence of red light that is amplified with this bias. The

photocurrent measured under back optical bias is comparable to the one measured without any bias due to the attenuation of the red signal and small amplification of the blue signal.

In the spatial region $\varepsilon + \varepsilon'$ the irradiation pattern is due to two LEDs. In the example of (Fig. 7a), the detector receives low frequency signals from red/green and blue/green emitters placed at the top (Fig. 5). Under front background light the photocurrent is enhanced when compared to the signal measured without background light, as the presence of the red and green light signals induces large photocurrent amplification. Under back background light, the photocurrent signal is similar the one measured without background, as there is a balance among the amplification factor due to the blue signal and the attenuation ($\alpha_F < 1$) from both red and green lights.

In the spatial region of type α (Fig. 7b) the detector receives signals from 3 LEDs, namely, from the low frequency blue/green emitter (top side) and from both red/green emitters (left side). Again, the optical excitation is caused by different wavelengths but at different frequencies. In the central position (β , Fig. 7c) the signal measured under back illumination is comparable to the signal measured without background illumination, which is due to the presence of both red and blue wavelengths that exhibit opposite behaviors under back illumination. The red light quenches the signal and the blue one amplifies it. On the other hand, the photocurrent under front illumination results in an amplified signal compared with the signal without optical background bias, due to the high amplification factor of the red light.

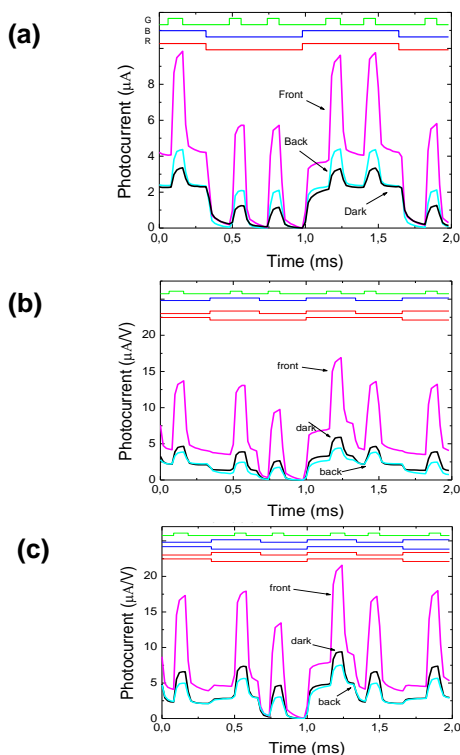


Fig. 7. Photocurrent measured without and under front and back optical bias in a spatial region of type: (a) $\varepsilon + \varepsilon'$, (b) α and β . At the top, it is shown the input modulated optical signals from red, blue and green emitters.

Decoding strategy

Based on the measured photocurrent an algorithm to automatically detect the position of the sensor in the spatial regions previously defined for the unit navigation cell as well as the identification of the unit navigation cell. Firstly, the green signal was extracted from the photocurrents. Secondly, the green signal was subtracted from the photocurrents. Then, the photocurrents signals under front and back bias were processed to evaluate the modulus of the complex Fourier coefficients. When the calculated coefficient is above a certain threshold the signal is considered to be present at the respective frequency. This procedure was implemented in an automatic process using MatLab to decode the location position of the detector. Fig. 8 shows the recovery of the signal transmitted by the green channel containing the identification of the unit navigation cells.

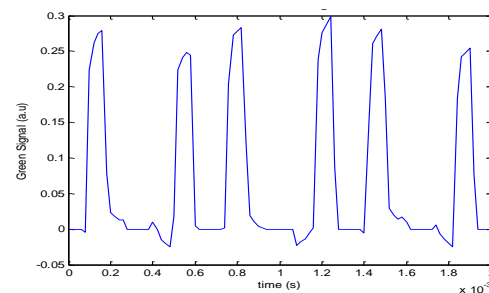


Fig. 8. Decode of the information transmitted by the green channel.

The modulus of the Fourier coefficients of the front and back photocurrents evaluated after the extraction of the green signal contribution is displayed in Table II. When the modulus of the Fourier coefficients of front and back photocurrents are balanced the photocurrent at that frequency is assigned to the red and blue light. In this case, a red and a blue emitter are simultaneously transmitting information at the same frequency. On the other hand, when the modulus of the Fourier coefficients of the front photocurrent is much higher than the correspondent coefficients of the back photocurrent, the photocurrent of that specific frequency is assigned to a red emitter. Alternatively, when the modulus of the Fourier coefficients of the back photocurrent is much higher than the coefficients of the front photocurrent, signal is allocated to a blue emitter.

Table II - Modulus of the Fourier coefficients of the front and back photocurrents.

	Frequency (Hz)	Fourier Coefficient	
		Front	Back
$\varepsilon + \varepsilon'$ (Q)	1500	0.586	0.303
	4500	0.203	0.111
α	750	2.420	1.270
	1500	2.170	0.416
	2250	0.607	0.309
	4500	0.770	0.149
β	750	0.474	0.249
	1500	0.575	0.299
	2250	0.114	0.057
	4500	0.204	0.110

Results show that in in position $\varepsilon+\varepsilon'$ the signals are transmitted at a single frequency of 1500 Hz, while in positions α and β the photocurrent exhibits 2 frequencies (750 and 1500 Hz). The analysis of the respective modulus of the Fourier coefficients shows that in position $\varepsilon+\varepsilon'$ the signals are due to the presence of both red and blue lights, which demonstrates that the photodetector is located at the north position within the navigation unit cell. In position α , the frequency 750 Hz is due a red and a blue light while frequency 1500 Hz is due to a red emitter. This corresponds to the southwest cardinal direction. For the central position, the modulus of the Fourier coefficients demonstrates, as expected, that the frequency 750 Hz is being transmitted by a red and a blue emitter, and the same at the frequency of 1500 Hz. The path of the detector, shown in the example of Figure 7, along the navigation unit cell extends from north to southwest and back to the central position.

Conclusions

In this paper, we present a VLC system for navigation purposes based on the wavelength and frequency of the emitted signals to decode the position of the detector. A theoretical study on the irradiation patterns is presented to support the position resolution of the proposed system.

Experimental results demonstrate the capability of the system. Future work will comprise a more detailed and complete description of the emitted light flux.

Acknowledgements

This work was sponsored by FCT – Fundação para a Ciência e a Tecnologia, within the Research Unit CTS – Center of Technology and systems, reference UID/EEA/00066/2013 and by projects IPL/2016/VLC_MIMO/ISEL and IPL/2017/SMART_VeDa/ISEL.

References

1. E. Ozgur, E. Dinc, O. B. Akan, *Physical Communication* 17 (2015) 72.
2. J. Armstrong, Y. Sekercioglu, A. Neild, *Communications IEEE*, 51(12) (2013) 68.
3. T. Sagotra, R. Aggarwal, *Interna. J. of Eng. Trends and Technology*, 4(3) (2013) 403.
4. Z. Zhou, M. Kavehrad, P. Deng, *Opt. Eng.* 51(8), (2012).
5. A. Jovicic, J. Li, T. Richardson, *Communications Magazine, IEEE*, 51(12) (2013) 26.
6. Louro, P., Vieira, M., Fernandes, M., Costa, J., Vieira, M.A., Caeiro, J., Neves, N., Barata, M., "Optical demultiplexer based on an a-SiC:H voltage controlled device", *Phys. Status Solidi C* 7, No. 3-4, 1188–1191 (2010)
DOI: [10.1002/pssc.200982702](https://doi.org/10.1002/pssc.200982702).
7. M. A. Vieira, M. Vieira, V. Silva, P. Louro "Optical signal processing for indoor positioning using a-SiCH technology" *Proc. SPIE* 9891, *Silicon Photonics and Photonic Integrated Circuits V*, 98911Z (May 13, 2016).
8. P. Louro; V. Silva ; J. Costa ; M. A. Vieira and M. Vieira, "Added transmission capacity in VLC systems using white RGB based LEDs and WDM devices ", *Proc. SPIE* 9899, *Optical Sensing and Detection IV*, 98990F (April 29, 2016).
9. Louro, P., Silva, V., Vieira, M.A., Vieira, M., "Viability of the use of an a-SiC:H multilayer device in a domestic VLC application", *Phys. Status Solidi C* 11, No. 11–12, 1703–1706 (2014).
DOI : [10.1002/pssc.201400035](https://doi.org/10.1002/pssc.201400035).

10. P. Louro, J. Costa, M. Vieira, M. A. Vieira, Y. Vygranenko, "Use of VLC for indoors navigation with RGB LEDs and a-SiC:H photodetector", *Proc. of SPIE*, vol 10231, *Optical sensors 2017* (102310F-2).
11. P. Louro, M. Vieira, M. Fernandes, J. Costa, M.A. Vieira, J. Caeiro, N. Neves, M. Barata, *Phys. Status Solidi C* 7(3–4), (2010) 1188.
12. M. Vieira, M. A. Vieira, I. Rodrigues, V. Silva, P. Louro, "Photonic Amorphous Pi'n/pin SiC Optical Filter Under Controlled Near UV Irradiation", *Sensors & Transducers*, Vol. 184, Issue 1, January 2015, pp. 123-129.